The effect of temperature and pressure on necking of polycarbonate*

S. Nazarenko, S. Bensason, A. Hiltner† and E. Baer
Department of Macromolecular Science and Center for Applied Polymer Research, Case Western Reserve University, Cleveland, OH 44106, USA

The effect of temperature and pressure on necking behaviour of polycarbonate was studied in tension. Following the concepts elucidated by Coates and Ward, neck geometry and neck propagation were related to the materials parameters: strain rate sensitivity and strain hardening parameter. The relationship between neck profile and the true stress–true strain curve was established by combining an analytical expression for the macroscale mechanics of the flow process with a constitutive equation describing the true stress, true strain and true strain rate dependence of the material. Having assumed a constitutive equation, the materials parameters were obtained from the stable neck geometry. The strain hardening parameter was found to be insensitive to changes in pressure and temperature in the range studied and had a value of approximately 3.3. Since the strain hardening parameter affected primarily the draw ratio, the latter was essentially independent of temperature and pressure. The increase in strain rate sensitivity parameter with pressure and decreasing temperature from 0.028 to 0.035 was manifest as a gradual broadening of the neck. The molecular significance of the materials parameters is discussed in terms of the contributions of two separate processes to plastic deformation: thermally activated yielding and the temperature and pressure independent stretching of a molecular network.

(Keywords: polycarbonate; yielding; necking)

INTRODUCTION

Many polymers, both amorphous and semicrystalline, are able to undergo large-scale plastic deformation in uniaxial tensile loading by necking and cold drawing. Following the plastic instability, identified with the maximum in the load–displacement curve, some polymers, unlike metals, develop a stable neck. It is the ability of polymers to strain harden that makes neck stabilization possible. Once stabilized, the neck propagates at a steady state along the specimen until the entire gauge length is stretched in the process known as cold drawing. In contrast to polymers, metals do not exhibit cold drawing since the neck in metals does not stabilize.

The relationship of neck geometry and neck propagation to the true stress (σ), true strain (ε), true strain rate ($\dot{\varepsilon}$) behaviour was recognized by Coates and Ward in an instructive series of papers in which an explanation for the widely differing neck geometries of polyethylene was sought[1–3]. On the condition that the neck propagates with a fixed profile, implying that each element of the material follows the same pathway across the true σ–ε–$\dot{\varepsilon}$ surface, these authors noted that the pathway is fixed by the strain hardening behaviour and the strain rate sensitivity, these being in effect the slopes of the true σ–ε–$\dot{\varepsilon}$ surface. These parameters depend on σ, ε, $\dot{\varepsilon}$, temperature and pressure to varying degrees depending on the material, and differences are reflected in such factors as sharpness of the neck and draw ratio achieved through the neck.

A material exhibiting a very high degree of strain hardening and also having a very high strain rate sensitivity will draw in a fairly uniform manner with only small evidence of necking. The other extreme is a material exhibiting a very low degree of strain hardening and also having a very low strain rate sensitivity. Such a material will neck sharply to high draw ratios, and possibly the neck will not stabilize, in which case the material will fail in the neck. In polymers, strain hardening effects are dominant and the strain rate sensitivity parameter is small. Furthermore, it is an important characteristic of many polymers, including polyethylene and poly(vinyl chloride), that the strain hardening parameter increases with strain in tensile loading[4,5]. This allows stabilization of the neck and makes it possible for polymers to draw to high extensions. This important feature differentiates polymers from ductile metals where, in contrast, the strain hardening parameter decreases with strain until the neck fractures, i.e. the neck is not stabilized.

One method to obtain the strain hardening parameter and strain rate sensitivity is based on determination of the true stress–true strain curve at several constant true strain rates[4]. This requires special instrumentation since, once necking begins, the extension rate must be closely controlled to maintain the true strain rate constant at the minimum diameter. The strain rate sensitivity can also be measured by other methods, such as stress relaxation or experiments with step change in strain rate[6]. None of these approaches is amenable to high pressure measurements. A simple approach used in the present

* Presented at 'Polymer Science and Technology—a conference to mark the 65th birthday of Professor Ian Ward FRS', 21–23 April 1993, University of Leeds, UK

† To whom correspondence should be addressed

0032-3861/94/18/3883–10

study makes it possible to determine the strain rate sensitivity and strain hardening parameter from the steady state neck profile, obtained in conventional constant crosshead speed tensile loading of cylindrical specimens with uniform cross-section. With this approach, the relationship between the neck profile and the true stress–true strain curve is established by combining an analytical expression for the macroscale mechanics of the flow process with a constitutive equation describing the true stress–true strain behaviour of the material. This approach was used to examine the effects of temperature and pressure on necking of polycarbonate (PC).

EXPERIMENTAL

Cylindrical tensile specimens of bisphenol A PC (Makrolon MPG 3408) were machined with a lathe from extruded rods with diameter of 12 mm. The uniform gauge section was 16 mm in length with a diameter of 3.8 mm and a fillet radius of 5.6 mm. After machining, specimens were carefully polished, first with fine grades of wet silicon carbide paper, followed by 5, 1 and 0.3 μm alumina powder. A 200 Å layer of gold was deposited through an electroformed nickel mesh with 500 wires per inch, to obtain a square grid pattern on the gauge portion of the specimen.

The hydrostatic pressure apparatus used in this study has been described in detail elsewhere[7]. It is a constant crosshead speed machine contained in a chamber filled with a pressure transmitting fluid, silicon oil (Dow Corning 200). The load is measured with a pressure compensating load cell, and the displacement by a linear variable differential transducer. The hydrostatic pressure during the experiment was maintained within ± 50 atm. The pressure chamber had two quartz viewing windows 7 mm in diameter: one was used to photograph the specimen during testing, the other was for illumination.

Tests were performed at room temperature at a crosshead speed of 0.5 mm min^{-1}. It is conventional to seal specimens in tests conducted in a high pressure fluid to prevent environmental effects on deformation and fracture behaviour. Comparison of stress–strain behaviour of sealed and unsealed specimens revealed that PC was not sensitive to these effects below 2.1 kbar. In order to monitor the specimen shape accurately during deformation, the specimens were not sealed.

Experiments at atmospheric pressure were performed with an Instron 1123 testing machine equipped with an environmental chamber. The effect of temperature on the deformation behaviour was studied between room temperature and -65°C. Low temperatures were attained by liquid nitrogen cooling. The testing speed was the same as with the high pressure tests. The specimen was photographed during all experiments, both at atmospheric and high pressures, with a Nikon 3F camera equipped with a telescopic lens. A typical photomicrograph obtained during loading (*Figure 1*) reveals the neck profile and the deposited gold mesh. The 6 mm length of the specimen in the field of view was sufficient to cover the complete neck profile at all temperatures and pressures.

Engineering stress–strain behaviour was determined from load–displacement data based on the initial specimen geometry. True stress and true strain were calculated from the diameter measured from micrographs obtained during the experiment. Assuming constant volume during

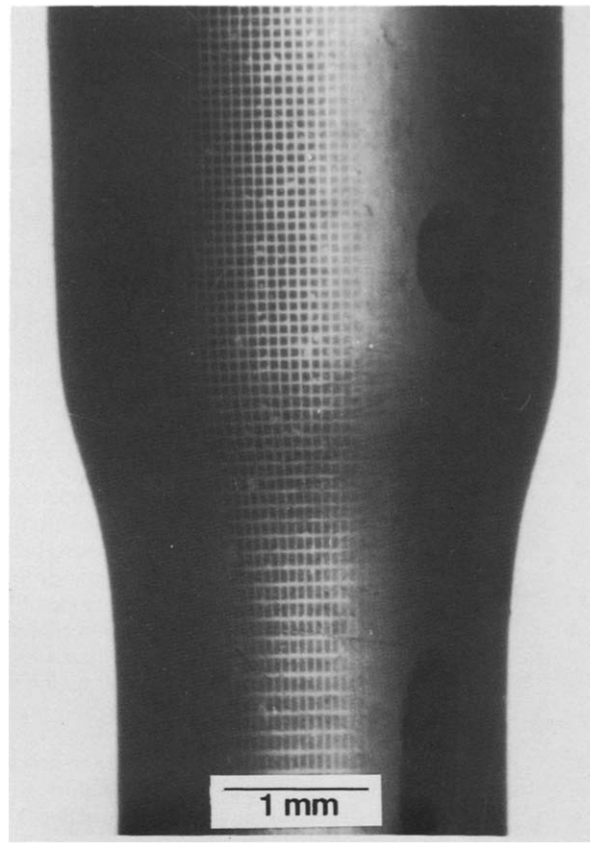

Figure 1 The steady state neck profile of PC at 21°C obtained during loading

deformation, the true strain was determined by:

$$\varepsilon_{true} = 2\ln\left(\frac{D_0}{D_i}\right) \quad (1)$$

where D_0 and D_i are the initial and instantaneous diameters, respectively. The true stress was based on the instantaneous cross-sectional area and was obtained by:

$$\sigma_{true} = \sigma_{eng}\left(\frac{D_0}{D_i}\right)^2 = \sigma_{eng}\lambda \quad (2)$$

This approach neglects the effects of stress triaxiality in the neck, and gives an average value of the stress across the neck.

The grid pattern was useful primarily to monitor the relative displacement of elements on the specimen. The true strain rate profiles were calculated from the true strain of particular elements on the grid in consecutive micrographs and the elapsed time.

RESULTS AND DISCUSSION

The engineering stress–strain behaviour

The engineering stress–strain curves obtained at various temperatures and pressures are shown in *Figures 2a* and *b*. Decreasing the temperature or increasing the pressure increased the elastic modulus, the yield stress and the yield strain. Following the yield point at the maximum in the stress–strain curve, a stress drop was observed when a diffuse neck formed. The sharpness of the stress drop, reflected in the negative slope of the curve following the maximum, lessened as the temperature decreased or the pressure increased. The effect was more pronounced in the pressure than in the temperature.

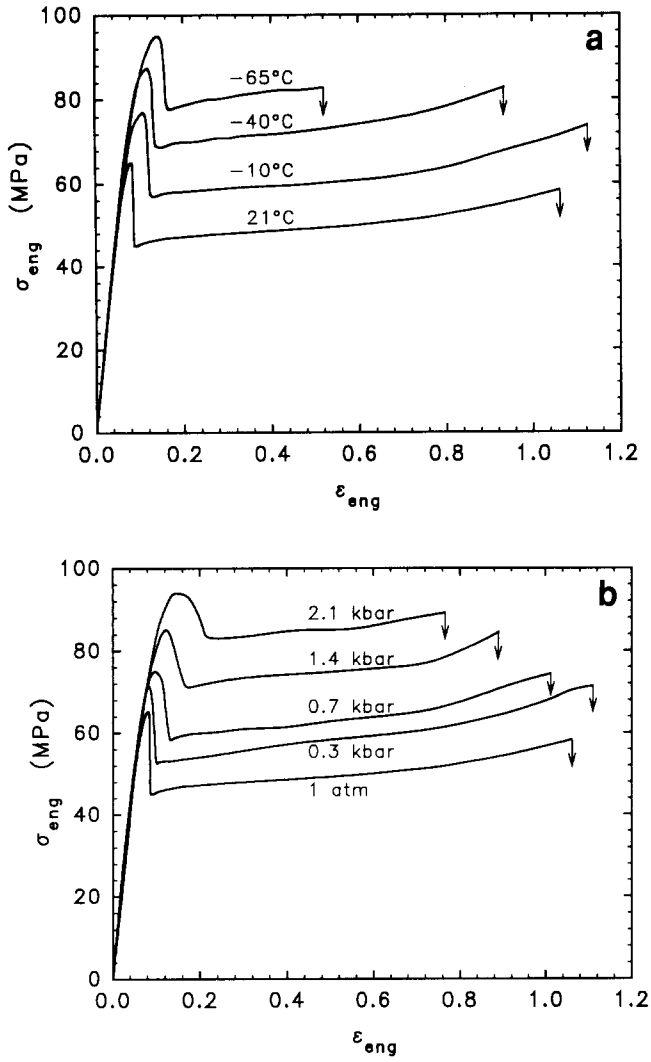

Figure 2 Engineering stress–strain curves: (a) as a function of temperature; (b) as a function of hydrostatic pressure

The yield stress, defined as the maximum in the engineering stress–strain curve, and the draw stress, defined as the plateau engineering stress following the stress drop, are plotted as a function of temperature and pressure in *Figures 3a* and *b*. Both the yield stress and the draw stress were linearly dependent on temperature and pressure. In the temperature range studied, the rates of change of the yield stress and draw stress with temperature were quite similar. In contrast, the draw stress increased faster than the yield stress with increasing pressure, a trend that has been observed previously[7,8].

The pressure dependence of the yield stress can be described by a modified von Mises yield criterion[7], written as:

$$\tau_{oct} = \tau_0 - \mu\sigma_m \tag{3}$$

where σ_m is the mean normal stress, τ_0 is the octahedral shear stress at $\sigma_m = 0$, and μ is a material parameter describing the pressure dependence of the yield stress. Calculating τ_{oct} and σ_m from relationships

$$\tau_{oct} = \frac{\sqrt{2}}{3}\sigma_y \tag{4}$$

and

$$\sigma_m = \frac{\sigma_y}{3} - P \tag{5}$$

(where P = hydrostatic pressure) a value of 0.06 was obtained for μ from the slope of the plot shown in *Figure 4*. This value is intermediate between the values of 0.072 and 0.047 reported by Christiansen *et al.*[7] and Mears and Pae[9], respectively.

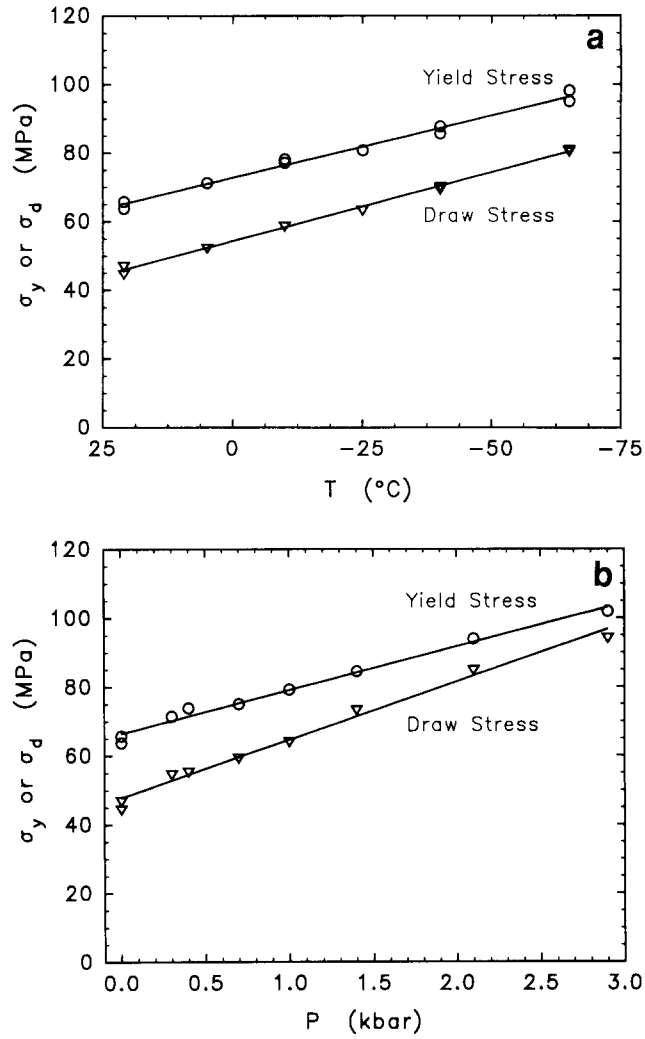

Figure 3 Engineering yield stress and engineering draw stress: (a) as a function of temperature; (b) as a function of hydrostatic pressure

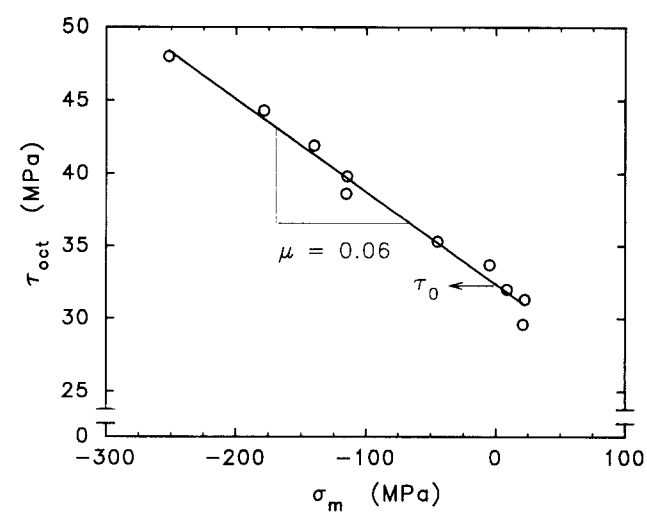

Figure 4 Plot of the octahedral shear yield stress as a function of the mean normal stress for the determination of μ

The true stress–true strain behaviour

The true stress–true strain curves obtained from cylindrical specimens usually describe the state at the minimum diameter. The point of minimum diameter, which was used to construct curve a in *Figure 5*, has a unique stress–strain–strain rate history. Once a neck initiates at the weakest point, the rest of the specimen contracts. Subsequently, points away from the instability follow a variety of other true stress–true strain paths. This is illustrated in *Figure 5* with the four pathways that are followed by points 1–4 in the schematic drawings. Curve a is followed by point 1 and corresponds to the conventional minimum diameter true stress–true strain curve. At the other extreme is the pathway followed by point 4, which is common to all points that are outside the region of neck formation. When the instability occurs, the true stress and strain relax via curve d to position D. Point 4 and points beyond leave position D one by one as the neck propagates steadily through the specimen; they follow the steady state true stress–true strain curve defined by the path DF. Points that are within the region of instability each follow a unique pathway that is intermediate between curves a and d. Two such pathways are illustrated: point 2 follows pathway b and joins the steady state curve at position B; similarly, point 3 follows pathway c, joining the steady state curve at position C. The dashed lines in *Figure 5* depict the true stress–true strain distribution of all the points along the specimen at various successive instances, t_1, t_2, t_3, during neck formation and stabilization.

In PC specimens with rectangular cross-section, instability usually occurs differently. Instead of diffuse necking characterized by an axially symmetric reduction in cross-sectional area that extends over an appreciable length of the specimen, instability occurs as a macroscopic shear band at an angle across the width of the specimen. Subsequently, the shear band evolves to a stable diffuse neck. The true stress–true strain state of the material during instability cannot be determined when the cross-section is rectangular. The only pathway that is measurable in this case is the steady state pathway DF[10].

An important consequence of necking is the development of true strain rate gradients. This is illustrated by the evolution of the true strain rate profile during neck formation shown in *Figure 6*. Before plastic instability, the true strain rate along the specimen was uniform and approximately equal to the engineering strain rate of 0.03 min^{-1}, as indicated by the dotted line. At instability, the strain rate rose rapidly at one point to a maximum

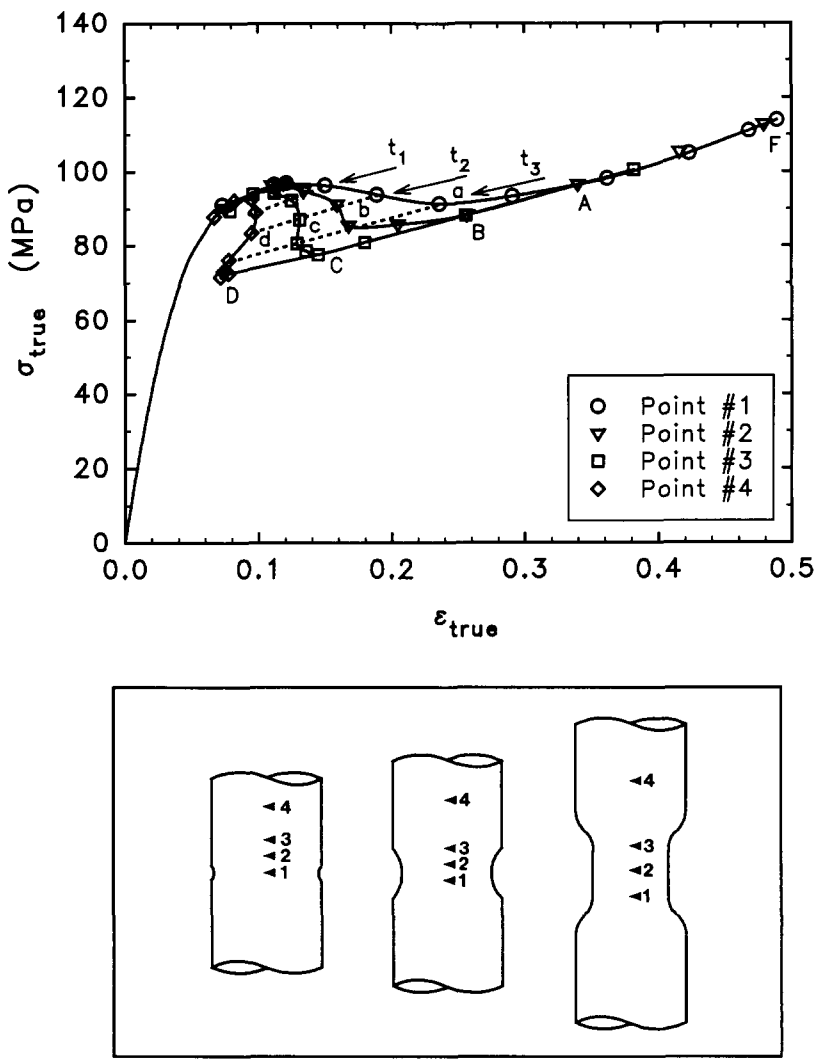

Figure 5 The true stress–true strain diagram at −40°C depicting the various true stress–true strain pathways encountered by various points on the specimen following instability

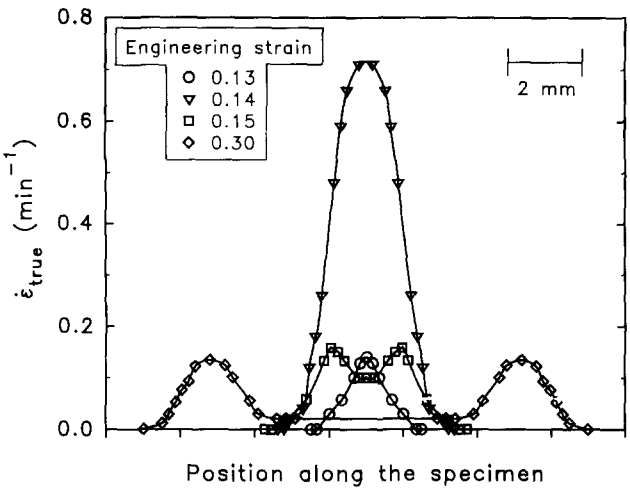

Figure 6 The time evolution of true strain rate distribution along the specimen at −40°C. The plot was obtained assuming symmetry of the two shoulder profiles around the point of instability

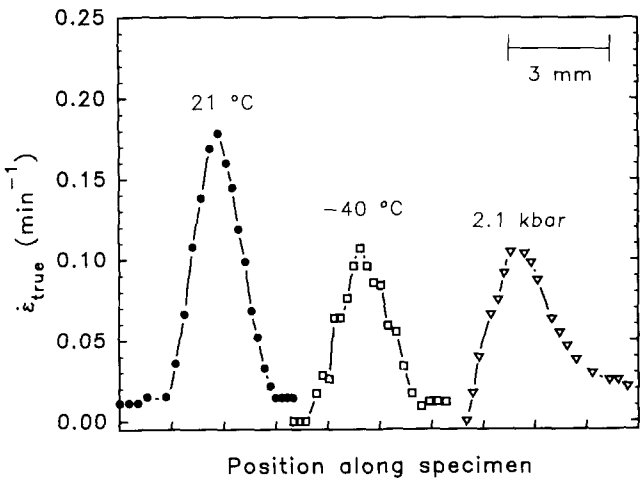

Figure 7 The comparison of true strain rate profiles across the neck propagating at steady state at 21°C, 1 atm; −40°C, 1 atm; 21°C, 2.1 kbar

value. The strain rate then decreased to the steady state profile. This profile subsequently moved in both directions as the neck propagated. Simultaneously the true strain within the neck increased at a very low rate.

The effects of temperature and pressure on the steady state true strain rate profile are illustrated in *Figure 7*. The decrease in maximum true strain rate with increasing pressure or decreasing temperature reflected broadening of the neck. The highest steady state value of 0.18 min^{-1}, about six times the engineering strain rate, was measured at 21°C and 1 atm pressure.

In order to describe the instability of PC, the general criterion for tensile deformation developed by Hart[11] was adopted. This approach is based on the strain hardening and strain rate sensitivity properties of the material. Defining a dimensionless strain hardening parameter γ as:

$$\gamma \equiv \frac{1}{\sigma}\left(\frac{\partial \sigma}{\partial \varepsilon}\right)_{\dot{\varepsilon}} \tag{6}$$

and the strain rate sensitivity parameter m as:

$$m \equiv \frac{\dot{\varepsilon}}{\sigma}\left(\frac{\partial \sigma}{\partial \dot{\varepsilon}}\right)_{\varepsilon} \tag{7}$$

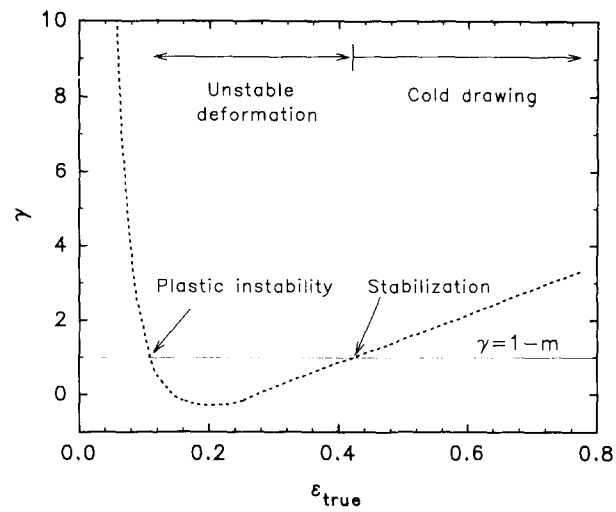

Figure 8 The variation of the strain hardening parameter as a function of true strain at −40°C. The horizontal line at the bottom with $\gamma = 1 - m$ represents the stability criterion developed by Hart

the stability criterion for uniform tensile deformation, as obtained by Hart, has the form:

$$\gamma + m - 1 \geqslant 0 \tag{8}$$

where a positive value of $(\gamma + m - 1)$ denotes a stable deformation state; equality is the condition for the transition from a stable to unstable state, or vice versa. The strain hardening parameter and the strain rate sensitivity parameter thus define the instability. When the strain rate sensitivity is omitted from consideration, equation (8) is equivalent to the Considere construction[12].

The strain hardening parameter can be obtained directly from the slope of the true stress–true strain curve. Assuming that m is much smaller than γ, the graphical presentation of the stability criterion of equation (8) for PC is shown in *Figure 8*. Initially, γ is large and decreases with increasing strain. When $\gamma = 1$, the deformation becomes unstable and a neck appears in the specimen. The neck grows thinner as the material continues to strain soften. Stabilization of the neck and subsequent cold drawing are only possible if the material develops enough strain hardening to overcome the instability criterion. In metals, the neck does not stabilize following instability since the strain hardening parameter continues to decrease until the neck fractures. In polymers, it is possible for the strain hardening parameter to increase following the instability[5], in which case the formation of a stable neck is observed when γ is again equal to 1. Once stabilized, the neck propagates with constant speed along the specimen in both directions by movement of the 'shoulders'.

Analytical description of stable neck propagation

The relationship between the neck profile and the true stress–true strain curve was established by combining an analytical expression for the macroscale mechanics of the flow process with a constitutive equation describing the true stress, true strain and true strain rate dependence of the material. Having assumed a constitutive equation, materials parameters were obtained from the neck geometry.

The problem of a geometric configuration travelling at steady state was solved for Lüders band propagation in metals by Hart[13]. Hart's model is general, and is also

applicable to other yielding phenomena. The model describes the steady state propagation of a narrow band of strain, in this case the Lüders band, along a specimen under constant load, until the entire specimen is strained by an amount corresponding to the maximum strain in the band. When it was recognized that stable neck propagation in ductile polymers exhibits the same macroscopic characteristics, this approach was also used to describe the neck shape in PC[14]. Hart's equation for the strain distribution along the Lüders band is based on the condition of static equilibrium at any position y along the specimen with cross-sectional area A, which is under load P:

$$P=\sigma(\varepsilon,\dot{\varepsilon})A \tag{9}$$

Then

$$0=\frac{dP}{dy}=A\left[\left(\frac{\partial\sigma}{\partial\varepsilon}\right)_{\dot{\varepsilon}}\left(\frac{d\varepsilon}{dy}\right)+\left(\frac{\partial\sigma}{\partial\dot{\varepsilon}}\right)_{\varepsilon}\left(\frac{d\dot{\varepsilon}}{dy}\right)\right]+\sigma\left(\frac{dA}{dy}\right) \tag{10}$$

It is assumed that the force P, acting on each discrete cross-sectional element normal to the central axis, is constant. This implies that the strain along the specimen is uniaxial. Incorporating the steady state assumption that every point of the Lüders band moves with a constant velocity v along the specimen, such that:

$$\dot{\varepsilon}=v(d\varepsilon/dy) \tag{11}$$

then equation (10) is written in the final form as:

$$\left(\frac{d^2\varepsilon}{dy^2}\right)=\frac{\sigma-\left(\frac{\partial\sigma}{\partial\varepsilon}\right)_{\dot{\varepsilon}}}{v\left(\frac{\partial\sigma}{\partial\dot{\varepsilon}}\right)_{\varepsilon}}\left(\frac{d\varepsilon}{dy}\right) \tag{12}$$

To predict the steady state neck profile from equation (12), a constitutive equation that formulates the dependence of the true stress on true strain and true strain rate in the form of

$$f(\sigma,\varepsilon,\dot{\varepsilon})=0 \tag{13}$$

is needed. G'Sell and Jonas[4] found that many ductile polymers in tension follow an empirical constitutive equation of the form

$$\sigma=K\exp\left(\frac{\gamma_0}{2}\varepsilon^2\right)\dot{\varepsilon}^m \tag{14}$$

where K is a constant, γ_0 is the strain hardening coefficient with the functional dependence $\gamma=\gamma_0\varepsilon$, and m is the strain rate sensitivity parameter, assumed here to be independent of strain.

It is possible to obtain the strain hardening parameter, γ, directly from the slope of the true stress–true strain curve, if the true strain rate is kept constant. Particularly in the region of plastic instability, the true strain rate is considerably higher than the average strain rate in a constant crosshead speed experiment. However, the true strain rate decreases during neck stabilization and, owing to the relatively low natural draw ratio of PC, the difference between the true stress–strain curve from the conventional constant crosshead speed experiment and the constant true strain rate curve is small during stable neck propagation. Therefore, it may be possible to use data obtained in conventional constant crosshead speed experiments in the analysis.

The strain hardening coefficient γ_0 in equation (14) is then readily available from a single true stress–true strain curve at a given temperature and pressure. However, direct determination of the strain rate sensitivity parameter m is more difficult. Although several methods are available[6], none is feasible at high pressure. However, m and γ_0 can be obtained from a single constant crosshead speed experiment by combining equation (14) with Hart's analysis of the neck shape.

By substituting the definitions of the strain hardening parameter, γ, and strain rate sensitivity, m, with the functional dependence $\gamma=\gamma_0\varepsilon$, equation (12) takes the final form of:

$$\left(\frac{d^2\varepsilon}{dy^2}\right)=\left(\frac{1}{m}-\frac{\gamma_0}{m}\varepsilon\right)\left(\frac{d\varepsilon}{dy}\right)^2 \tag{15}$$

This equation is independent of time since it describes the steady state. The solution of this differential equation with proper boundary conditions gives $\varepsilon(y)$ which can be converted to $R(y)$, the radius profile of the steady state propagating neck.

Equation (15) was solved numerically by using the simplified Runge–Kutta method. This iterative procedure is based on reducing a second order differential equation to two first order differential equations. The boundary conditions for equation (15) were $\varepsilon=0$ and $d\varepsilon/dy=0$ at $y=0$. To start the iteration scheme, the initial strain gradient was chosen as 0.01. The longitudinal axis was scaled with the initial diameter, $D_0=2R_0$.

It is useful to illustrate the effects of m and γ on the true stress–true strain curves and the corresponding neck profiles. The effects of m and γ on the true stress–true strain behaviour calculated from equation (14) are illustrated in *Figures 9a* and *b*. This constitutive equation describes the uniaxial deformation of a plastic body and therefore does not predict the elastic behaviour and the instability region of the stress–strain curve. The values of the materials parameters m and γ_0 were chosen from the range that subsequently fitted the experimental data. The constant K was chosen as 70 MPa, approximately the value for PC at room temperature. Increasing strain rate sensitivity parameter m caused only a slight downward shift in the true stress–true strain curve, without affecting the shape. Increasing the strain hardening coefficient γ_0 caused a change in the shape of the stress–strain curves, with an increase in curvature particularly at high strains.

The corresponding neck profiles were generated by solving equation (15) and are shown in *Figures 10a* and *b*. The strain rate sensitivity parameter m mainly affected the sharpness of the neck; the effect on the draw ratio was insignificant. Increasing the strain rate sensitivity parameter produced a longer neck. The strain hardening parameter γ_0 had a major effect on the draw ratio, and thereby changed the sharpness of the neck as well. Although the length of the neck was not affected significantly by γ_0, the apparent sharpness of the neck was reduced when increasing the strain hardening coefficient resulted in a lower draw ratio.

Based on these observations, γ_0 in this study was expected to be fairly constant, since the draw ratio in the neck was not affected significantly by temperature or pressure. However, since the neck was observed to get shallower and longer at lower temperatures and higher pressures, m was expected to increase with increasing pressure and decreasing temperature.

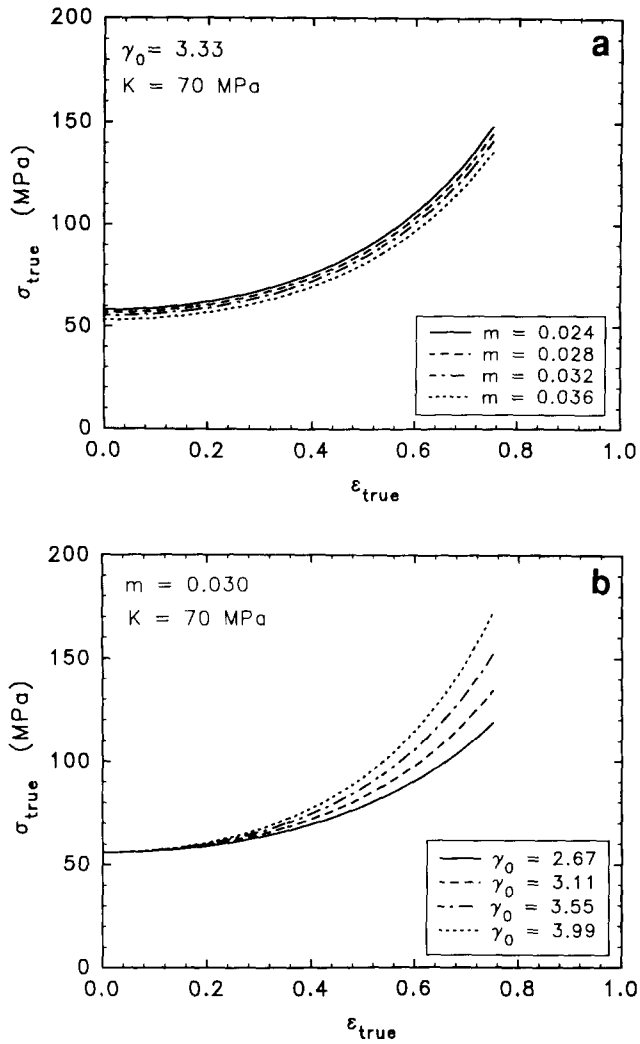

Figure 9 (a) The variation of the true stress–true strain curves obtained by the constitutive equation as a function of m at constant γ_0 and K ($\gamma_0 = 3.33$, $K = 70$ MPa). (b) The variation of the true stress–true strain curves obtained by the constitutive equation as a function of γ_0 at constant m and K ($m = 0.030$, $K = 70$ MPa)

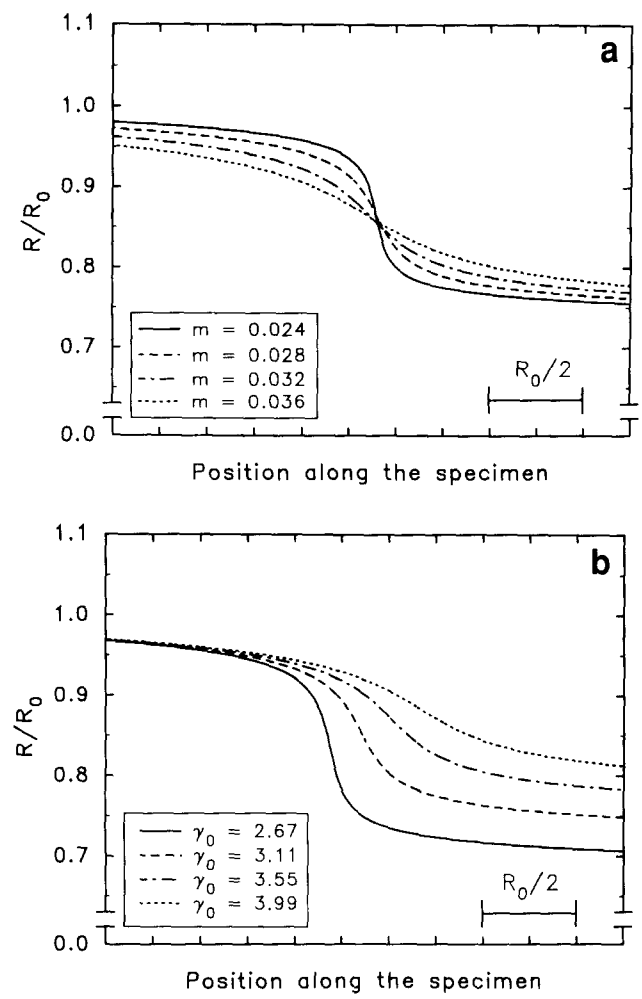

Figure 10 (a) The calculated neck profiles for the true stress–true strain curves of *Figure 9a* with $\gamma_0 = 3.33$. (b) The calculated neck profiles for the true stress–true strain curves of *Figure 9b* with $m = 0.030$

Since m and γ_0 affect the neck profile independently, it was possible to determine these parameters for each temperature and pressure from a micrograph of the neck during steady state propagation by using an iterative fitting procedure. Starting with an approximate value for γ_0, first a fit to the draw ratio was obtained. Next, m was varied to obtain the best fit to the shoulder profile. Fine readjustments of both γ_0 and m were made until the best fit to the overall profile was obtained. Examples of the best fit to the neck profile are shown in *Figure 11*. The values of γ_0 and m obtained by the fitting procedure are listed in *Table 1*.

As expected, the strain hardening coefficient was insensitive to variations in pressure and temperature and had a value of approximately 3.3. In contrast, the strain rate sensitivity parameter was affected both by pressure and temperature. As a function of temperature, m increased from 0.028 at room temperature to 0.033 at -65°C. The strain rate sensitivity parameter increased with pressure to 0.035 at 2.1 kbar. The resultant m values are plotted as a function of temperature and pressure in *Figure 12*. The increase was not a linear function of pressure or temperature, but instead m appeared to level off at higher pressures and lower temperatures.

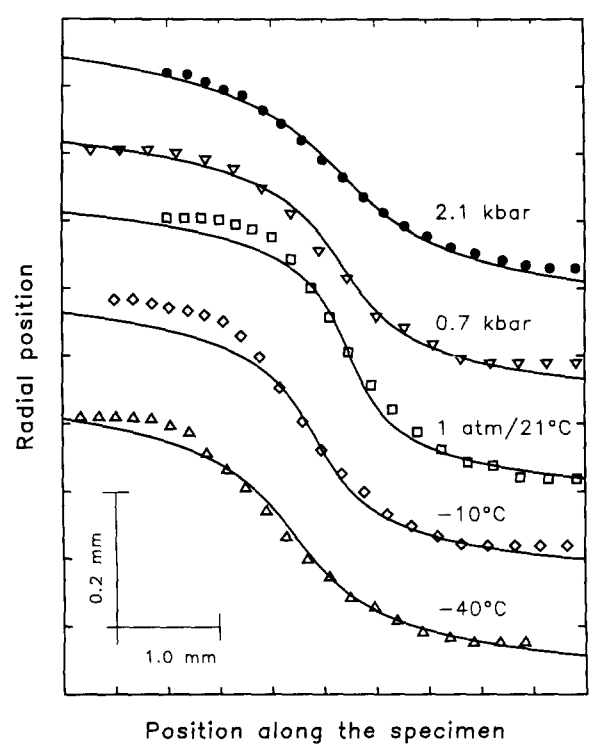

Figure 11 The comparison of experimental stable neck profiles at various temperatures and pressures with calculated neck profiles (symbols indicate the experimental data points)

Table 1 The values of strain rate sensitivity parameter m, strain hardening coefficient γ_0, and K as a function of hydrostatic pressure and temperature

Condition	m	γ_0	K (MPa)
Hydrostatic pressure (kbar)			
0.001	0.028	3.33	62
0.7	0.032	3.33	82
1.4	0.034	3.33	102
2.1	0.035	3.33	125
Temperature (°C)			
21	0.028	3.33	62
5	0.030	3.25	72
−10	0.031	3.33	81
−25	0.031	3.33	87
−40	0.033	3.33	98
−65	0.033	3.45	113

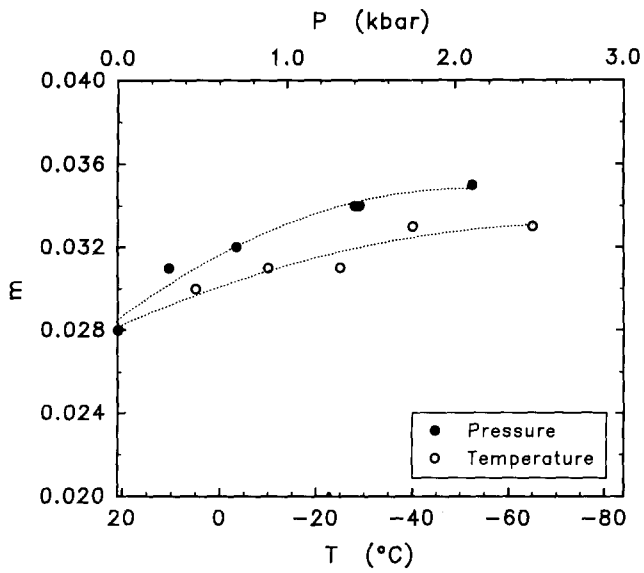

Figure 12 The strain rate sensitivity parameter as a function of temperature and hydrostatic pressure

The values of m and γ_0 were inserted into the constitutive equation (14) and K was obtained by adjusting the curves vertically to give the best fit. The resultant K values are also listed in *Table 1*. The calculated true stress–true strain curves are compared with experiment in *Figures 13a* and *b*. The solid symbols are data points that correspond to minimum diameter measurements at various positions on the engineering stress–strain curve. The K values were obtained by fitting these data points. The open points in *Figure 13* were obtained by measurements from a single micrograph of the neck profile during steady state neck propagation. The most left-hand point corresponds to the state of the unnecked material during neck propagation. The slight deviation of these points is a manifestation of non-uniformity of the state of stress and strain through the neck.

Molecular aspects of plastic deformation

The phenomenological approach that considers plastic deformation to consist of the contributions of two separate processes, thermally activated yielding and stretching of a molecular network[15,16], can relate the parameters m and γ to molecular aspects of plastic deformation[17]. Within this framework, the thermal activation formalism is used to explain the temperature, pressure and strain rate dependence of yielding, whereas the molecular network contributes to the increasing resistance to further plastic stretching. Thus, conceptually, the strain rate sensitivity parameter accommodates the thermally activated yield process, and the strain hardening coefficient reflects the contribution of the molecular network.

The specific contribution of these two processes can be determined from the true stress–true strain curve by conveniently defining the 'steady state' activated yield stress, σ^*, as the point of intersection of the extrapolated strain hardening portion with the initial pre-instability region. This treatment removes the transient effects related to instability from consideration. Temperature, pressure and strain rate all affect σ^*.

The shear activation volume Ω_A can be obtained from experiments at different strain rates as:

$$\Omega_A = kT\left(\frac{\partial \ln \dot{\varepsilon}}{\partial \tau^*}\right)_{T,P} \tag{16}$$

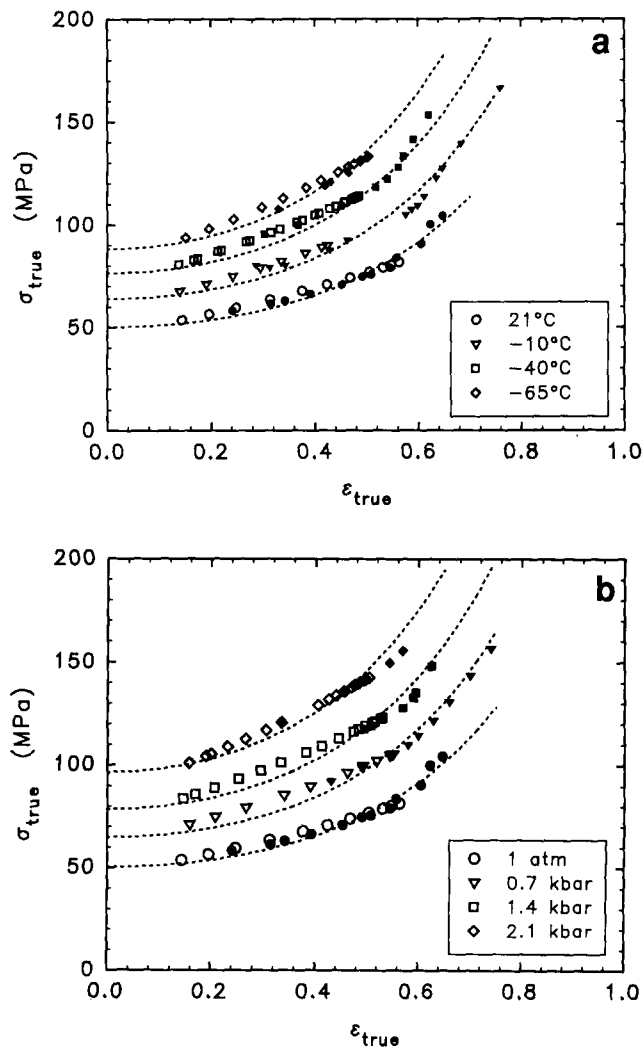

Figure 13 The comparison of true stress–true strain data points obtained from experiments with the behaviour predicted by the constitutive equation: (a) at various temperatures; (b) at various hydrostatic pressures (open symbols are data points obtained from a single micrograph along the neck; filled symbols measured from the minimum diameter at various engineering strains; dashed line obtained from the constitutive equation)

where k is the Boltzmann constant and

$$\tau^* = \frac{1}{\sqrt{3}}\sigma^* \tag{17}$$

Alternatively, the strain rate sensitivity parameter can be incorporated into equation (16), with the result that m can be expressed as a function of two activation parameters, τ^* and Ω_A:

$$m = \frac{kT}{\tau^*\Omega_A} \tag{18}$$

It is characteristic of polymers that τ^* and Ω_A have opposite dependences on temperature and pressure. These dependences are shown in *Figures 14a* and *b* for PC, where τ^* and Ω_A were calculated from equations (17) and (18). Whether m increases or decreases with temperature and pressure is not obvious from the trends in τ^* and Ω_A. For PC, m increased then gradually levelled off with pressure, while the opposite has been reported for polyethylene[18]. It is anticipated that this would cause the neck in polyethylene to become sharper with pressure.

The increasing resistance to stretching during cold drawing in polymers has been associated with the gradual orientation of the macromolecules. It is observed that the strain hardening behaviour is dependent on the state of strain[19]. Thus the constitutive law describing plastic deformation of PC in shear is different from that in tension. In shear, γ is strain independent[19], while in this study a strain-dependent γ was needed in tension and a linear functionality was found to be satisfactory.

The strain hardening coefficient was approximately independent of temperature and pressure in the range studied for PC. This was consistent with the phenomenological model[15], which assumes that the molecular network is not affected by changes in temperature and pressure. As a consequence, the draw ratio of PC remained almost constant, while the variation of the steady state neck profile with pressure and temperature reflected the effect of pressure and temperature on the strain rate sensitivity parameter.

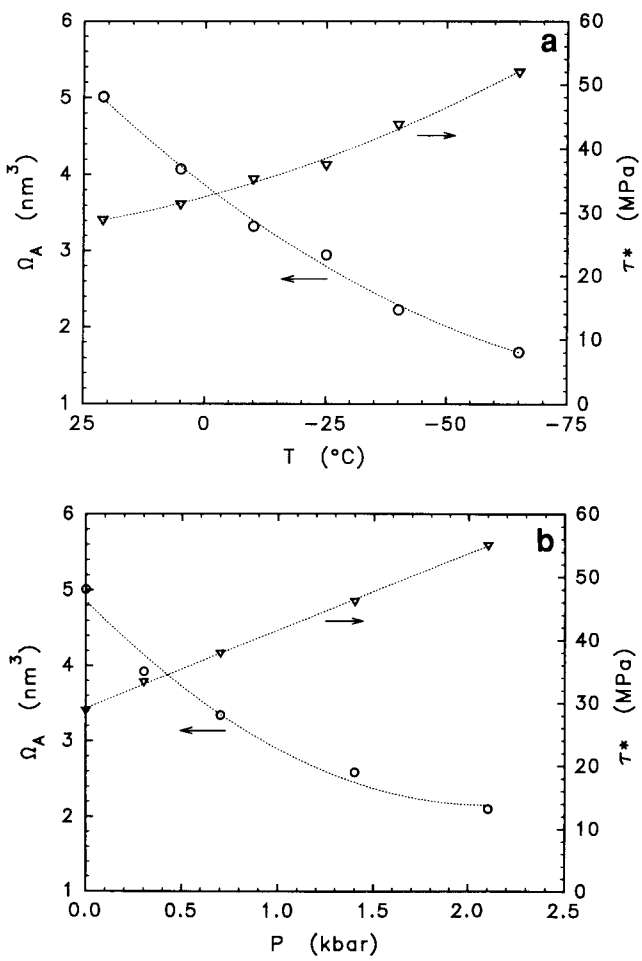

Figure 14 The variation of the shear activation volume and the shear activation stress: (a) as a function of temperature; (b) as a function of hydrostatic pressure

SUMMARY

The effect of temperature and hydrostatic pressure on the uniaxial deformation behaviour of polycarbonate was studied. In the temperature and pressure range extending from room temperature and atmospheric pressure to −65°C and 2.9 kbar, the true stress–true strain behaviour was determined, with particular emphasis on the effects of these external variables on the neck geometry. The draw ratio in the neck was measured as approximately 1.7, independent of hydrostatic pressure and temperature. Unlike the draw ratio, the sharpness of the neck was affected considerably: increasing pressure and decreasing temperature produced longer and shallower neck profiles.

The true stress–true strain behaviour following neck stabilization was described by a constitutive equation based on the strain hardening parameter and the strain rate sensitivity. The correspondence between these two materials parameters describing plastic deformation and the geometry of the stable neck was established by incorporating the constitutive equation into an analytical expression for the macromechanics of stable neck propagation. Based on this correspondence, changes in the stable neck shape and the draw ratio in the neck as a function of pressure and temperature were directly transformed to the temperature and pressure dependence of the strain hardening parameter and the strain rate sensitivity. This greatly simplified the experimental procedure for determining these parameters.

The strain hardening parameter was found to be insensitive to changes in pressure and temperature in the range studied and had a value of approximately 3.3, whereas the strain rate sensitivity parameter increased with pressure and decreasing temperature from 0.028 to 0.035. Using the Eyring formalism that treats yielding as an activated rate process, the shear activation volume was obtained from the strain rate sensitivity parameter and the activated yield stress. A decrease in shear activation volume was observed with increasing pressure and decreasing temperature. The results were also interpreted within the framework of a model that distinguishes between the effects of thermally activated yielding and stretching of a molecular network in plastic deformation. The constant strain hardening coefficient confirmed the insensitivity of the molecular network to pressure and temperature, while the strain rate sensitivity, reflecting the thermally activated shear process, was affected by changes in temperature and pressure.

ACKNOWLEDGEMENT

This work was generously supported by the National Science Foundation grant no. DMR 91-00300.

REFERENCES

1 Coates, P. D. and Ward, I. M. *J. Mater. Sci.* 1980, **15**, 2897
2 Coates, P. D. and Ward, I. M. *J. Mater. Sci.* 1978, **13**, 1957
3 Coates, P. D., Gibson, A. G. and Ward, I. M. *J. Mater. Sci.* 1980, **15**, 359
4 G'Sell, C. and Jonas, J. J. *J. Mater. Sci.* 1979, **14**, 583
5 G'Sell, C. in 'Plastic Deformation of Amorphous and Semi-crystalline Materials' (Eds B. Escaig and C. G'Sell), Les Editions de Physique, Les Ulis, 1982
6 Padmanabhan, K. A. and Davies, G. J. 'Superplasticity', Springer Verlag, Berlin 1980, p. 29
7 Christiansen, A. W., Baer, E. and Radcliffe, S. V. *Phil. Mag.* 1971, **24**, 451
8 Spitzig, W. A. and Richmond, O. *Polym. Eng. Sci.* 1979, **19**, 1129
9 Mears, D. R. and Pae, K. D. *J. Polym. Sci. B* 1969, **7**, 349
10 Buisson, G. and Ravi-Chandar, K. *Polymer* 1990, **31**, 2071
11 Hart, E. W. *Acta Metall.* 1967, **15**, 351
12 Vincent, P. I. *Polymer* 1960, **1**, 7
13 Hart, E. W. *Acta Metall.* 1955, **3**, 146
14 Robertson, R. E., General Electric Research Laboratory, Report No. 64-RL-3794C, Schenectady, New York, 1964
15 Haward, R. N. and Thackray, G. *Proc. R. Soc. (London) Ser. A* 1968, **302**, 1973
16 Argon, A. S. *Phil. Mag.* 1973, **28**, 839
17 Ward, I. M. *Polym. Eng. Sci.* 1984, **24**, 724
18 Davis, L. A. and Pampillo, C. A. *J. Appl. Phys.* 1971, **42**, 4659
19 G'Sell, C. and Gopez, A. J. *J. Mater. Sci.* 1985, **20**, 3462